



Photocatalytic decomposition of VOCs by AC–TiO₂ and EG–TiO₂ nanocomposites

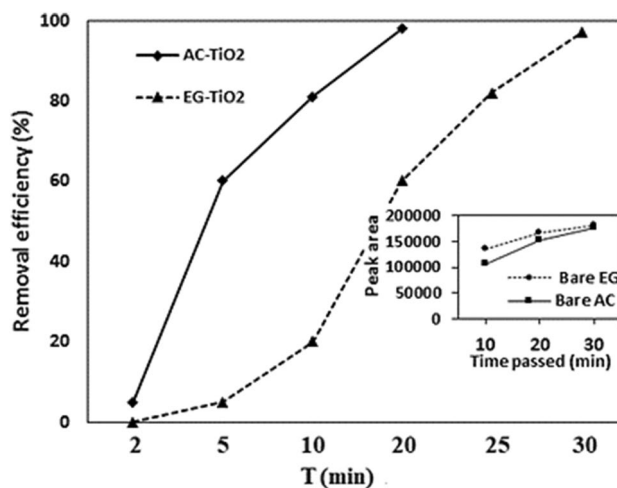
Babak Jaleh¹ · Mastaneh Gandomi Rouzbahani¹ · Kamaladdin Abedi^{2,3} · Saeid Azizian⁴ · Hossein Ebrahimi⁵ · Mahmoud Nasrollahzadeh⁶ · Rajender S. Varma⁷

Received: 21 February 2019 / Accepted: 23 April 2019 / Published online: 29 April 2019
© Springer-Verlag GmbH Germany, part of Springer Nature 2019

Abstract

In this study, TiO₂ nanoparticles (NPs)-based catalysts were prepared for the photocatalytic removal of toluene as a model VOC from air under UV light. Expanded graphite (EG) and activated carbon (AC) as two sustainable supports were employed for immobilization of TiO₂ NPs by sol–gel technique. In this approach, substrates were added to TiO₂ sol–gel and heated up to 60 °C followed by calcination process at 400 °C to afford, EG/TiO₂ and AC/TiO₂. The studies show that much better results ensued for AC–TiO₂ because of higher surface area, good nanoparticle distribution, and lower pore width. The products were characterized by X-ray diffraction, scanning electron microscope, energy dispersive X-ray, as well as N₂ adsorption/desorption.

Graphical abstract



Keywords AC/TiO₂ · EG/TiO₂ · Characterization · Photocatalyst · VOCs

- ✉ Babak Jaleh
jaleh@basu.ac.ir
- ✉ Mahmoud Nasrollahzadeh
mahmoudnasr81@gmail.com
- ✉ Rajender S. Varma
varma.rajender@epa.gov

Extended author information available on the last page of the article

Introduction

Volatile organic compounds (VOCs) such as toluene, benzene, xylene, etc. are a group of hydrocarbons emitted from building materials, furnishings, and many industrial processes that are greatly harmful to environment and human (Vandenbroucke et al. 2011; Ojala et al. 2011). Despite their deleterious effects, VOCs are still widely produced, used,

and released to the atmosphere (Ojala et al. 2011). This issue has been a major concern for many researchers in recent decades, and they have tried to find efficient and cost-effective technologies for the removal of these compounds from the gas and water streams (Varshney et al. 2016; Pelaez et al. 2013; Virkutyte and Varma 2010; Virkutyte et al. 2010; Virkutyte and Varma 2012a, b; Virkutyte et al. 2012).

Recently, noble metal and metal oxides have been broadly applied for the elimination of VOCs due to their high thermal, chemical, and physical stabilities, high efficiency and activity, large surface area, and strong electron transfer abilities (Park et al. 2019; Sharma et al. 2019). Despite all the advantages, the catalytic activity was decreased due to the agglomeration of the nanoparticles. In fact, the nanoparticles used in the reaction, due to their very small size, cannot be recovered and remain in the reaction environment and caused various constraints. Therefore, to address this problem, heterogeneous catalysts have been developed that include stable support such as carbon nanotubes (CNTs), graphene, Al_2O_3 , Fe_3O_4 , etc. to stabilize the nanoparticles (Goudarzi and Salavati-Niasari 2018; Mahdiani et al. 2017, 2018; Salavati-Niasari and Bazarganipour 2007, 2008, 2009; Salavati-Niasari et al. 2010; Nasrollahzadeh et al. 2018, 2019a, b).

There has been a great deal of interest in oxidation processes using nanoparticle catalysts specially titanium dioxide (TiO_2) in many scientific and industrial fields (Yang et al. 2009; Narayanaswamy et al. 2008). This unique semiconductor has attracted considerable attention (Choi et al. 2006; Verma et al. 2016) and has been shown to be one of the most suitable catalysts, having a strong oxidation activity. Moreover, its significant attributes such as chemical inactivity, low cost, non-toxic nature, compatibility with the environment, along with long-term stability and a lower energy band gap (3.02 eV) enabled many practical applications (Wang and Zhou 2011; Yap et al. 2011; Vega et al. 2011). Anatase, rutile, and brookite are prominent phases of TiO_2 among which anatase and rutile have been primarily involved in environmental decontaminations (Williams and Kamat 2009). Anatase is usually found to be more active than rutile, but in recent years, the scientific literature suggests that the photocatalytic and photovoltaic properties of mixed phases of TiO_2 nanoparticles are much preferred as compared to pure anatase TiO_2 , reducing electron-hole recombination (Wetchakun and Phanichphant 2008).

In order to improve specific surface area of TiO_2 and its affinity toward VOCs molecules (due to the polar structure of the most semiconductors), and thereby attaining much higher activities, attention has been focused to coat it on adsorbent matrixes such as silica, zeolites, as well as carbon-structured materials (Colmenares et al. 2016, 2017) such as activated carbon (AC) and expanded graphite (EG); among these, AC and EG are considered as exceptional supports

(Abedi et al. 2015a; Zarezade et al. 2011; Wang et al. 2009a; Arana et al. 2003). Thanks to the unique molecular structure, extremely high affinity for the most of VOCs, large surface area, microporous structure, availability in various forms and sizes, high adsorption capacity, and low cost, AC can be an ideal substrate (Ghaedi et al. 2011). EG has also a porous structure with typical apparent densities of $0.002\text{--}0.01\text{ g cm}^{-3}$ and has been used in wide-ranging practical applications in many fields such as hydrogen storage, sensors production, catalytic oxidation, biomedical treatment, as well as adsorption (Zhao and Liu 2009). In recent years, the ecological problems arising from the oil spills in the world have caused EG to be considered as a strong and powerful adsorbent for water contaminants (Yue et al. 2010). Tsumura et al. studied the effect of TiO_2 on decomposition of absorbed heavy oil and found that doping anatase-type TiO_2 onto EG could markedly accelerate the decomposition of heavy oil under UV irradiation (Tsumura et al. 2002).

Adsorption has long been used as one of the most successful methods for air and water treatment. However, it does not mineralize the pollutants but simply prevents them from further recycling in the atmosphere. There also exists the problem of saturation and breakthrough with the adsorption process. Combining the both techniques, adsorption and the catalytic oxidation, has been proposed as a hybrid method to overcome some of the drawbacks and thriving performance for the removal of contaminants (Abedi et al. 2015b; Lee et al. 2004; Wang et al. 2009b; Sharma et al. 2019). Furthermore, magnetic, electrochemical, and photocatalytic properties of catalyst can be modified throughout coating some material (Goudarzi and Salavati-Niasari 2018; Mahdiani et al. 2017; Salavati-Niasari and Bazarganipour 2009).

Consequently, during this work, TiO_2 nanoparticles were synthesized using sol-gel technique, and carbon-based adsorbents, i.e., activated carbon, and expanded graphite were deployed as supports for TiO_2 . The study focused on the synthesis and characterization of AC- TiO_2 and EG- TiO_2 nanocomposites using XRD, SEM, EDX, and BET; the photocatalytic efficiency of AC- TiO_2 and EG- TiO_2 was investigated under UV radiation for mineralization of toluene as a model compound.

Materials and methods

General

Expandable graphite powder with 300 μm diameter and 30 μm thickness was supplied by Beijing Invention Biology Engineering and New Material Co., China. Activated charcoal having granules with the mean diameter of 1.5 mm was purchased from Merck, Germany. Tetra *n*-butyl titanate [$\text{Ti}(\text{O}i\text{Bu})_4$] used as Ti precursor, PrOH , and acetyl acetone

(with purity of 99.8%) as solvent, and toluene (with purity higher than 99%) used as air pollutant, were all obtained from Merck, Germany.

Expanded graphite was prepared using expandable graphite powder which was dried at 90 °C for 12 h, followed by heating up to 1050 °C for just 15 s.

The surface state and structure of the composites were observed by scanning electron microscopy (SEM) (Scam MV 2300, Cam type). Chemical characterization of the prepared nanostructures was also analyzed by dispersive X-ray spectroscopy (EDX). The crystalline nature of the samples was investigated by X-ray diffractometer (Philips powder diffractometer type PW 1373 goniometer) with Cu K α ($\lambda = 1.5405 \text{ \AA}$) radiation source. The diffraction patterns were recorded in the 2θ range of 10°–60° with scanning speed of 2° min⁻¹. The BET surface area was determined using the N₂ adsorption data in the relative pressure (P/P_0) range of 0.05–0.5 at 77 °K using a BELSORP-max nitrogen adsorption apparatus (Japan Inc.). Furthermore, the desorption isotherm was used to determine the pore size distribution using the density functional theory (DFT) method.

A quartz cylindrical glass tube with 3 cm diameter and 30 cm length was employed as a catalyst reactor. Some amount of glass wool was applied each time at both ends of the tube in order to prevent particles escaping from the inlet and outlet of the reactor. In the center of the reactor, an 8-W lamp with wavelength of 253.7 nm (Philips TUV 8 W/G8 T5 Bulb), 15 mm \times 300 mm, was placed axially as a UV radiator. The distance between the lamp and the reactor wall was filled by EG-TiO₂ or AC-TiO₂ nanocomposites. The setup system consisted of several parts including air supply, air drying, air cleaning, air controlling and measuring, pollutant injection, mixing, decomposition, and analysis sections. A compressor was used to supply normal air in order to dilute the pollutant molecules. This air was subjected to flow through our experimental setup and controlled using several regulators and needle valves. It was then allowed to flow through a ceramic-activated carbon and a cellulosic ester filter to be cleaned from water vapor and any background air contaminants. Afterward, the toluene liquid was injected into the line as air pollutant (300 ppm) through a specified port using a motor-driven syringe pump (SP-510, JMS), from where it was allowed to be mixed inside a mixing chamber and could be accessed from the reactor. A temperature controller was used to keep the temperature of the system at 40 °C, making it possible for the liquid substance to vaporize conveniently. All the setup system was inspected to be thoroughly gastight.

After the steady state conditions were established, the effluent gas was sampled and subjected to analysis using a gas chromatograph (GC/FID, Shimadzu-2010), equipped with a SGE capillary column with the inner diameter of 0.22 mm, film diameter of 0.25 μ m, and length of 25 m. A

Varian 3800 GC equipped with a Saturn 2200 mass spectroscopy system (GC/MS), with the same column mentioned above, was also used during our experiments. Temperature programming with both GCs was as follows: 80 °C for 1 min and then increased by 12 °C min⁻¹ up to 180 °C and finally kept constant there for 5 min. 100 μ l of effluent gas was removed each time using a sampling syringe.

During all experiments, the UV lamp was turned on for 20 min after steady state conditions and then the removal efficiency was analyzed.

Preparation of TiO₂

TiO₂ particles were prepared through modified sol-gel process using tetra *n*-butyl titanate as the precursor. Ti(OBu)₄ was diluted with PrOH as solvent, and the resultant mixture was stirred at room temperature for 1 h. Acetylacetonate (AcAc) as stabilizer was added dropwise to the mixed solution under stirring, and the resultant mixture stirred for another 2 h. Afterward, HNO₃ aqueous solution (2 or 3 droplets of HNO₃ in 1.8 ml of H₂O) was added under stirring to ensure that the pH of sol-gel solution maintained around 2. Finally, the solution was heated under reflux at 75 °C for 8 h to obtain a colorless crystalline sol. At this stage, the temperature was kept constant and strictly controlled to avoid instant gelation. The volume ratios of PrOH, H₂O, and AcAc to Ti(OBu)₄ were 40, 100, and 1, respectively (Hu et al. 2009).

Preparation of AC-TiO₂ and EG-TiO₂ nanocomposites

For the preparation of AC-TiO₂ and EG-TiO₂ nanocomposites, AC and EG were firstly added to TiO₂ sol followed by subjecting the mixtures to sonication in an ultrasound bath for 30 min and the contents were maintained at room temperature for 2 days. Afterward, the mixtures were filtered and then dried at 60 °C for 5 h. The samples were finally calcined at 400 °C for 2 h. The flowcharts of TiO₂ sol, AC-TiO₂, and EG-TiO₂ nanocomposites, in terms of preparation procedure sequences, are presented, in Fig. 1a–c, respectively. Image of synthesized materials was taken by digital camera and included in Fig. 2.

Results and discussion

The EG-TiO₂ and AC-TiO₂ nanocomposites were synthesized and then characterized using several techniques in order to determine how the structure of composites affects their catalytic activity under UV irradiation. It has been recognized in the literature that the catalytic activity of a catalyst can be influenced by many factors such as adsorption

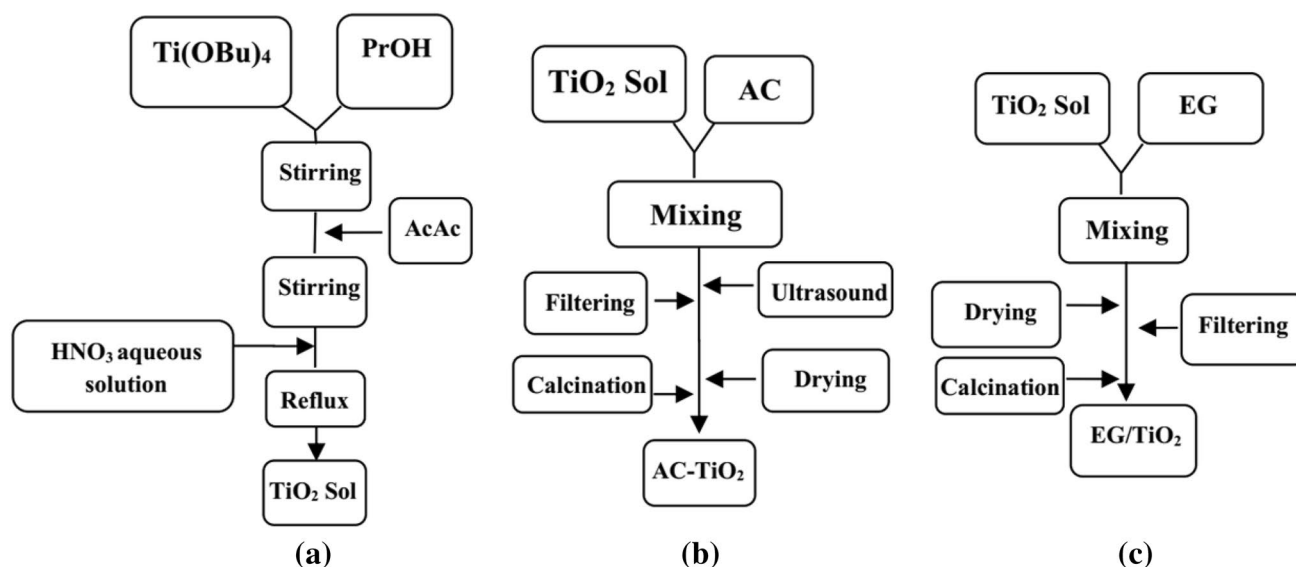


Fig. 1 Flowchart of preparation of **a** TiO₂ sol-gel, **b** AC-TiO₂ nanocomposite, **c** EG-TiO₂ nanocomposite

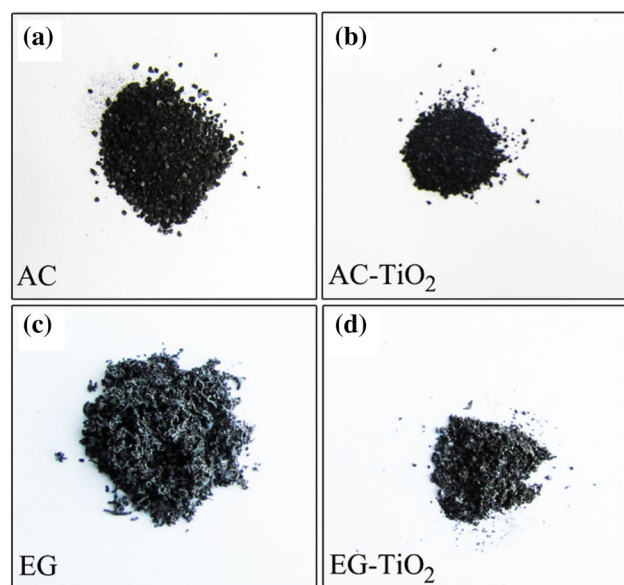


Fig. 2 Digital camera images of **a** AC, **b** AC-TiO₂, **c** EG, **d** EG-TiO₂ nanocomposite

properties and surface area of the substrate, Ti amount, pore size, TiO₂ crystalline phase etc. (Arana et al. 2003; Jafari et al. 2011; Jaleh and Shahbazi 2014; Yu et al. 2002). In keeping with these reports, the synthesis and characterization of EG-TiO₂ and AC-TiO₂ complexes were carried out.

Surface analysis of composites

The morphologies of EG and AC, before and after TiO₂ coating, are provided in Fig. 3. Lamellar structure of EG

is shown in Fig. 3a, and the pore structure of EG is found to be distributed uniformly, having a large number of thin and flat layers. The loaded TiO₂ particles could also be clearly observed over the EG substrate in Fig. 3b. The particles are in nano-scale range but have different shapes and sizes as depicted in Fig. 3b, the dispersion and distribution of TiO₂ particles being not uniform. Zhang et al. (2005) reported that more reactive sites can be expected in catalysts with higher particle distribution degrees. It can also be seen from the figure that the morphology of EG after TiO₂ coating was dramatically changed; some of the thin layers disappeared, joining and sticking together. The surface macroscopic alteration can be attributed to two factors; the wet process of sol-gel technique and the calcinations temperature. Due to the soft and fragile nature of EG, the sol-gel wet process can affect its structure adversely, reducing the surface area significantly. Although the calcination process can positively influence catalyst properties, it can also be considered as a detrimental factor for catalyst substrate and even catalyst phase transition (Ao and Lee 2005). In Fig. 3c, AC has a relatively smooth surface, having many holes and cavities along it. However, after deposition and calcination, TiO₂ particles are well attached and dispersed over the AC surface, making it much uniform and smooth (Fig. 3d). The distribution of TiO₂ particles over AC is also more uniform as compared to EG surface. According to Afanasov et al. (2009), the distribution pattern can have a considerable impact on the pollutant removal efficiency, since the contaminant molecules firstly adsorbed on substrate surface and then transferred to the nanoparticles for decomposition.

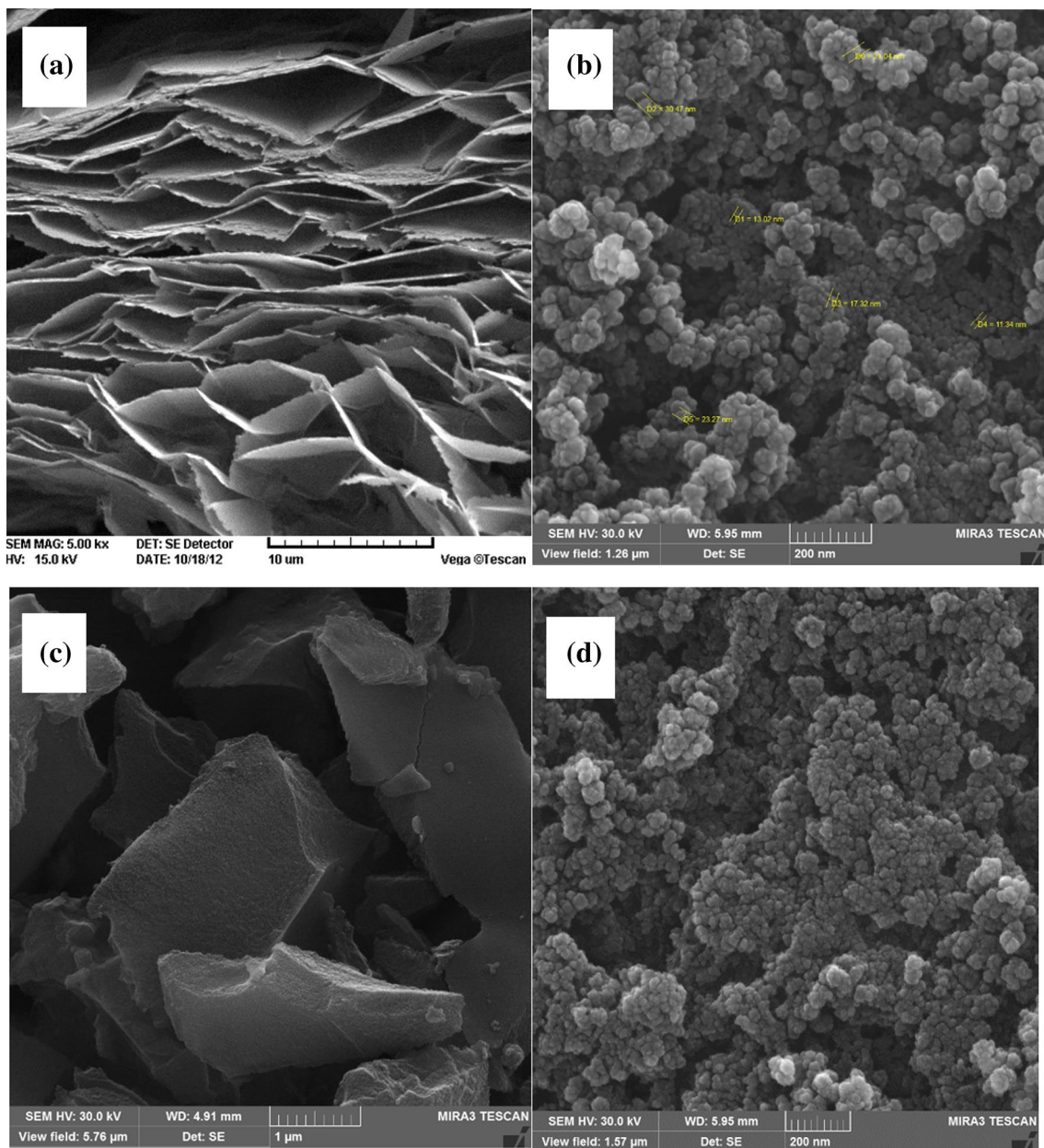


Fig. 3 SEM image of a EG, b EG-TiO₂, c AC, d AC-TiO₂

Elemental and pore size analysis

A quantitative EDX spectrum was obtained using SEM-EDX line scan technique to determine the elemental composition of samples. The analysis provides the percent by weight (wt%) and the percent number of atoms (at.%) of each identified element which are listed in Table 1 for EG-TiO₂ and AC-TiO₂. The results show that the nanocomposites comprise C, O, and Ti. Carbon atoms are the dominant element in both EG-TiO₂ and AC-TiO₂ samples accompanied by the O atoms in the second place followed by the minor quantities of Ti and with no detection of any

Table 1 EDX elemental composition of EG-TiO₂ and AC-TiO₂

	Element	Weight%	Atomic%
EG-TiO ₂	C	84.63	89.44
	O	12.29	9.75
	Ti	3.08	0.82
	Total	100.00	100.00
AC-TiO ₂	C	78.33	84.18
	O	18.57	14.98
	Ti	3.10	0.84
	Total	100.00	100.00

other impurity. Surprisingly, nearly the same amount of Ti was detected in both EG–TiO₂ and AC–TiO₂, which was not supported by the primary examination of SEM images (Fig. 3b, d); aggregation may well be the reason for this discrepancy. A significant shrinkage has been observed in EG structure after exposing to the wet medium of sol–gel, leading the TiO₂ particles to be accumulated on some parts of EG surface. Furthermore, as Table 1 shows, the % of O was also different in the two nanocomposites, much higher in AC–TiO₂. According to Szymański et al. (2002), substrate surface carboxylic groups can strongly participate in catalytic destruction of hydrocarbons (Abedi et al. 2014). Therefore, an optimum concentration of O would be highly valued.

The samples were also subjected to nitrogen adsorption–desorption measurements in order to characterize the pore structures of two nanocomposites, and results are shown in Fig. 4; all samples, e.g., EG, EG–TiO₂, AC, and AC–TiO₂ display an IV-type isotherm accompanied by the presence of hysteresis loops, indicating mesoporous structure patterns. The BET specific surface area and the total pore volume of bare substrates and nanocomposites are shown in Table 2.

As expected, the volume of AC–TiO₂ is slightly lower than that of AC, indicating the deposition of TiO₂ onto the template pores. For EG–TiO₂, this volume reduction was more noticeable which can be explained by the EG shrinkage as a result of introduction into the aqueous medium of sol.

The pore size distribution of samples was calculated by density functional theory (DFT) method (Fig. 5), which totally supported the BET results. From Fig. 5, it can be concluded that TiO₂ coating can lead to the pore width reduction especially for EG–TiO₂. It appears that all points of the two

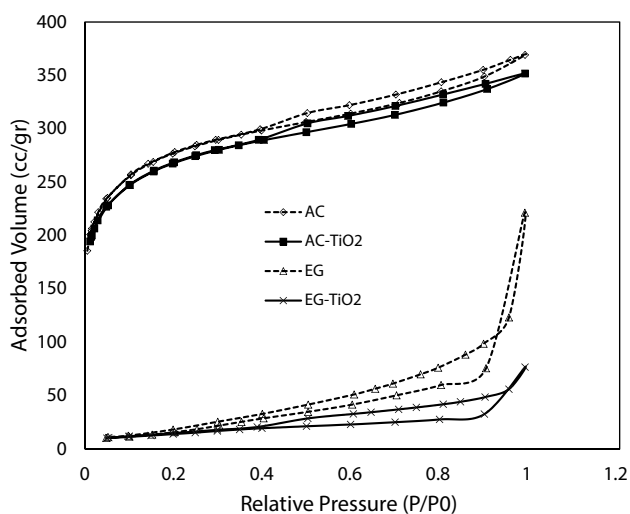


Fig. 4 N₂ adsorption–desorption isotherm of AC, AC–TiO₂, EG, and EG–TiO₂

Table 2 Specific surface area and total pore volume of EG, EG–TiO₂, AC, and AC–TiO₂

Sample name	EG	EG–TiO ₂	AC	AC–TiO ₂
Specific surface area (m ² g ⁻¹)	99.27	54.9	969.1	935.2
Total pore volume (cc g ⁻¹)	0.3425	0.1185	0.5724	0.5453

curves (AC and AC–TiO₂) coincide in the Fig. 5, implying no deposition of TiO₂ into AC, but with a magnification view, a difference of 135–190 nm appears between the two curves which can be attributed to a thin layer of TiO₂ nanoparticles. The pore width for EG–TiO₂ obtained in the range between 4 and 25 nm, while the distribution was much less for AC–TiO₂ (1–8 nm). The last result can strongly affect the catalytic activity rate.

Structural analysis

Figure 6 presents the X-ray diffraction patterns of some selected samples. The diffractogram shows the characteristic peaks of EG ($2\theta = 26.4^\circ$), and AC ($2\theta = 26$) which were accompanied by a mixture of anatase and rutile TiO₂ peaks in different amounts, locating at $2\theta = 25.1^\circ, 37.6^\circ, 47.7^\circ, 54.8^\circ, 59.8^\circ$, and $2\theta = 27.1^\circ, 41.0^\circ, 62.6^\circ$, respectively. An overlap is seen from Fig. 6 between the main peak of AC and that of anatase TiO₂ at $2\theta = 25.1$ corresponding to the (101) plane, which is also considered to be the main peak of TiO₂. Due to the presence of substrate species and also badly crystallized TiO₂, a non-smooth diffractogram shape was obtained for all samples. According to Addamo et al. (2004), the phase type and properties of nanoparticles depend

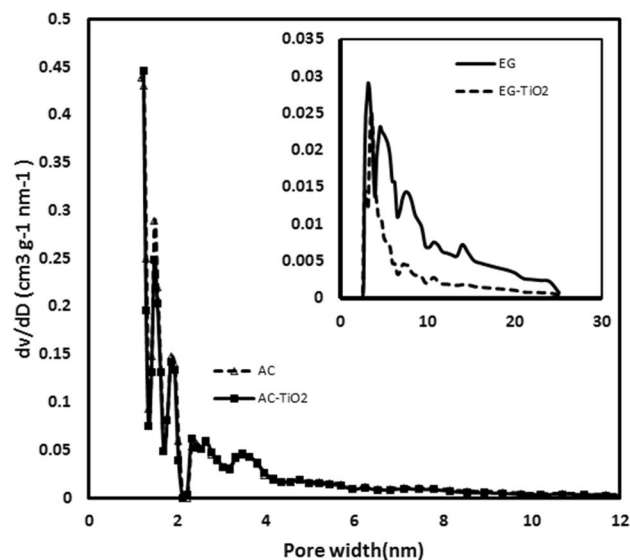
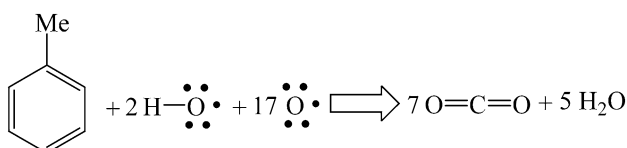
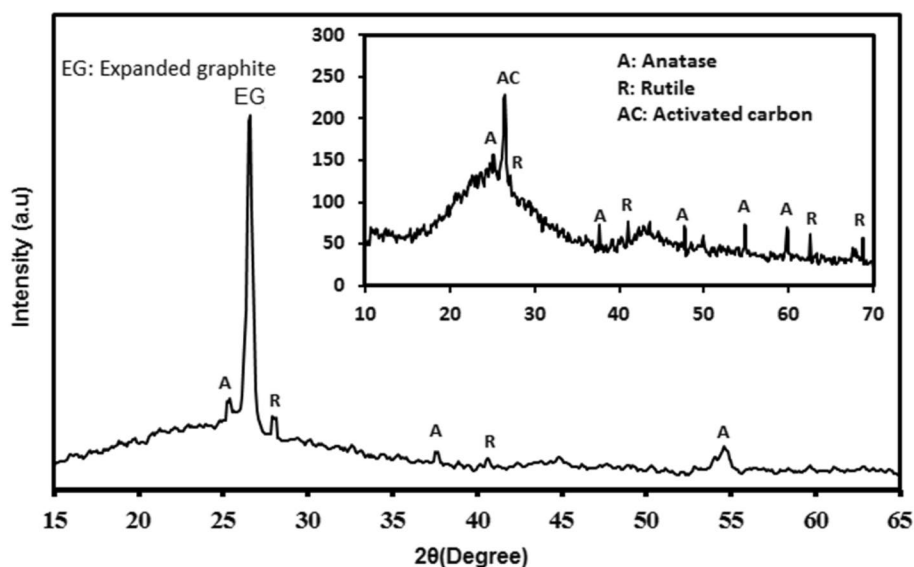


Fig. 5 DFT pore size distribution plot of EG, EG–TiO₂, AC, and AC–TiO₂

Fig. 6 XRD patterns of EG-TiO₂ and AC-TiO₂**Fig. 7** Possible pathway for toluene mineralization

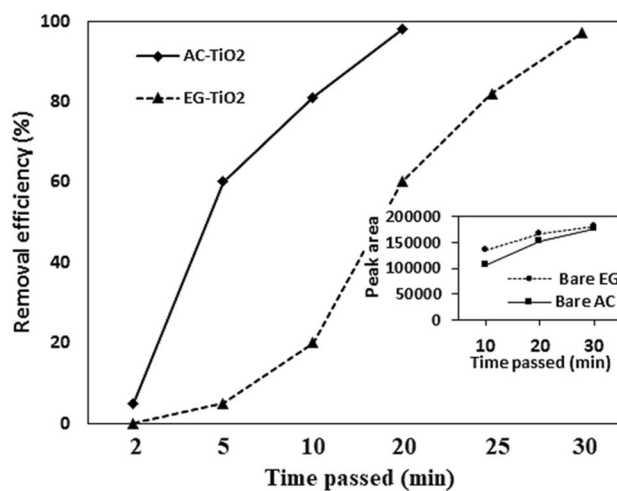
strongly on preparation conditions such as sol preparation sequence and calcination temperature; calcination temperatures higher than 400 °C may specially lead to the formation of much better crystallized anatase TiO₂. But, at the same time, higher temperatures result in higher aggregation and thereby reducing surface area of nanoparticles and also loss of TiO₂ surface hydroxyl groups which is fully destructive for catalytic activities.

Toluene mineralization

The effect of catalyst was investigated on toluene conversion in the presence of UV light, and our investigations were performed with both bare substrates and substrates coated by TiO₂.

Assuming the production of CO₂ and H₂O, as well as oxygen and hydroxyl radicals as dominant agents in toluene mineralization, the possible pathway is depicted in Fig. 7.

Figure 8 shows the photocatalytic activity of EG/TiO₂ and AC/TiO₂ for the degradation of toluene as a function of time; a relatively low activity was observed in removal efficiency (RE) after 2 min of UV radiation, and it then picked up after 5 min, rocketing by almost 60% for AC/TiO₂. Furthermore, in the presence of AC/TiO₂ total oxidation of toluene was obtained at 20 min of UV exposure. As far as the EG/TiO₂ is concerned, the first signs

**Fig. 8** Toluene removal efficiency over AC-TiO₂ and EG-TiO₂ as a function of temperature, and toluene breakthrough over bare AC and bare EG as a function of passed time

of activation appeared after 5 min under UV radiation, and no catalytic behavior is seen from the figure at lesser times. From this point onwards, a gradual enhancement was observed in the catalytic activity, and nearly the total decomposition of toluene was achieved after 30 min.

As can be seen from Fig. 8, AC/TiO₂ catalyst was more active relative to EG/TiO₂ which may be attributed to the stronger adsorption ability of AC. As Fig. 8 represents, prior to TiO₂ impregnation, the toluene breakthrough was much higher with the bare EG, indicating the greater capacity of AC to adsorb toluene. This may be more significant with prepared catalysts because the structure of EG/TiO₂ appeared to be much denser compared to the structure of bare EG, meaning a lower surface area for

EG/TiO₂, while no significant change occurred with the AC after impregnation.

It has been widely recognized that catalyst support can influence the catalytic performance significantly (Ao and Lee 2003; Ao et al. 2008). Ao and Lee (2003) prepared TiO₂ anatase loaded on AC and used it as catalyst for decomposition of phenols wherein phenol compounds were adsorbed on AC initially and then moved to the surface of TiO₂ continuously which improved the catalytic oxidation remarkably. In agreement with this, our findings also showed that the effect of catalyst template can be significant, and a high level of catalytic activity was observed during the present work. The damaging effects of calcination could be counteracted by higher rates of adsorption and providing more organic compounds close to nanoparticles as well as the dispersion of TiO₂ particles on the surface of AC (Li et al. 2007).

A strong relationship was observed between the time and removal efficiency (RE), and the trend for RE is obviously upwards in all cases regardless of the catalyst type (Fig. 8). Total oxidation of toluene was obtained after 20 min and 30 min with AC/TiO₂ and EG/TiO₂, respectively. Compared to the earlier studies (Schmidt-Szałowski et al. 2011; Yang et al. 2010; Zeng et al. 2010), much lesser time is needed to reach a stable and high catalyst activity, especially using AC/TiO₂. Notably, the level of activation with AC/TiO₂ was considerably high at 5 min, while no significant activity was observed with EG/TiO₂. This can be probably explained by the thorough dispersion of nanoparticles over AC surface as confirmed by SEM. As we surmised previously, a good distribution of TiO₂ particles was obtained on AC, while the pattern for EG was sporadic and was not much favorable. With higher quantities of nanoparticles dispersion over the substrate, much more hydroxyl groups could be available for redox reactions (Mul et al. 2001). Furthermore, a greater degree of aggregation estimated for EG/TiO₂ can be another reason for its lower RE.

Conclusion

The EG–TiO₂ and AC–TiO₂ were successfully prepared by sol–gel method with the morphology for EG and AC, as observed by SEM analysis, being lamellar and smooth, respectively; TiO₂ was well deposited on the surface of substrates. The XRD analysis confirmed that TiO₂ supported on carbon bases contains two different phases: anatase and rutile. Moreover, the EDX analysis showed that the elements are C, O, and Ti and no other elemental impurities were discerned. AC–TiO₂ showed a high catalytic activity, and nearly 100% of toluene was converted on its surface after 20 min of UV radiation. The catalytic activity of EG–TiO₂ was very strong after 30 min, while not appreciable at lesser exposure times. We anticipate this study will help

researchers design the appropriate preparative procedure and its processing, including calcination to attain the desirable traits for supported TiO₂.

Acknowledgements The authors would like to thank the physics department of Bu-Ali Sina University for the financial support.

Compliance with ethical standards

Conflict of interest The authors confirm that no conflict of interest arise with regard to the research leading to this paper, nor with publication of this work.

References

- Abedi K, Ghorbani-Shahna F, Jaleh B, Bahrami A, Yarahmadi R (2014) Enhanced performance of non-thermal plasma coupled with TiO₂/GAC for decomposition of chlorinated organic compounds: influence of a hydrogen-rich substance. *J Environ Health Sci Eng* 12:119
- Abedi K, Ghorbani-Shahna F, Bahrami A, Jaleh B, Yarammadi R (2015a) Effect of TiO₂–ZnO/GAC on by-product distribution of CVOCs decomposition in a NTP-assisted catalysis system. *Pol J Chem Technol* 17:32–40
- Abedi K, Ghorbani-Shahna F, Jaleh B, Bahrami A, Yarahmadi R, Haddadi R, Gandomi M (2015b) Decomposition of chlorinated volatile organic compounds (CVOCs) using NTP coupled with TiO₂/GAC, ZnO/GAC, and TiO₂–ZnO/GAC in a plasma-assisted catalysis system. *J Electrostat* 73:80–88
- Addamo M, Augugliaro V, Dipaola A, García-López E, Loddo V, Marci G, Molinari R, Palmisano L, Schiavello M (2004) Preparation, characterization, and photoactivity of polycrystalline nanostructured TiO₂ catalysts. *J Phys Chem B* 108:3303–3310
- Afanasov I, Shornikova O, Avdeev V, Lebedev O, Van Tendeloo G, Matveev A (2009) Expanded graphite as a support for Ni/carbon composites. *Carbon* 47:513–518
- Ao C, Lee S (2003) Enhancement effect of TiO₂ immobilized on activated carbon filter for the photodegradation of pollutants at typical indoor air level. *Appl Catal B Environ* 44:191–205
- Ao C, Lee S (2005) Indoor air purification by photocatalyst TiO₂ immobilized on an activated carbon filter installed in an air cleaner. *Chem Eng Sci* 60:103–109
- Ao Y, Xu J, Fu D, Shen X, Yuan C (2008) Low temperature preparation of anatase TiO₂-coated activated carbon. *Colloids Surf A Physicochem Eng Asp* 312:125–130
- Arana J, Doña-Rodríguez J, Rendón ET, Icabo CG, González-Dí O, Herrera-Melián J, Perez-Pena J, Colón G, Navá J (2003) TiO₂ activation by using activated carbon as a support: part I. Surface characterisation and decantability study. *Appl Catal B Environ* 44:161–172
- Choi H, Kim YJ, Varma RS, Dionysiou DD (2006) Thermally stable nanocrystalline TiO₂ photocatalysts synthesized via sol–gel methods modified with ionic liquid and surfactant molecules. *Chem Mater* 18:5377–5384
- Colmenares JC, Varma RS, Lisowski P (2016) Sustainable hybrid photocatalysts: titania immobilized on carbon materials derived from renewable and biodegradable resources. *Green Chem* 18:5736–5750
- Colmenares JC, Varma RS, Nair V (2017) Selective photocatalysis of lignin-inspired chemicals by integrating hybrid nanocatalysis in microfluidic reactors. *Chem Soc Rev* 46:6675–6686

- Ghaedi M, Tavallali H, Montazerzohori M, Mousavi SD, Khodadoust S, Soyak M (2011) A novel nanometer pore size acorn based activated carbon modified with 2-(4-methoxybenzylideneamino) thiophenol for the preconcentration of copper and zinc ions and their determination in some food samples. *Fresen Environ Bull* 20:2785–2793
- Goudarzi M, Salavati-Niasari M (2018) Using pomegranate peel powders as a new capping agent for synthesis of CuO/ZnO/Al₂O₃ nanostructures: enhancement of visible light photocatalytic activity. *Int J Hydrog Energy* 43(31):14406–14416
- Hu CY, Xu YJ, Duo SW, Zhang RF, Li MS (2009) Non-covalent functionalization of carbon nanotubes with surfactants and polymers. *J Chin Chem Soc* 56:234–239
- Jafari S, Azizian S, Jaleh B (2011) Adsorption kinetics of methyl violet onto TiO₂ nanoparticles with different phases. *Colloids Surf A Physicochem Eng Asp* 384:618–623
- Jaleh B, Shahbazi N (2014) Surface properties of UV irradiated PC-TiO₂ nanocomposite film. *Appl Surf Sci* 313:251–258
- Lee DK, Kim SC, Cho IC, Kim SJ, Kim SW (2004) Photocatalytic oxidation of microcystin-LR in a fluidized bed reactor having TiO₂-coated activated carbon. *Sep Purif Technol* 34:59–66
- Li Y, Zhang S, Yu Q, Yin W (2007) The effects of activated carbon supports on the structure and properties of TiO₂ nanoparticles prepared by a sol-gel method. *Appl Surf Sci* 253:9254–9258
- Mahdiani M, Sobhani A, Salavati-Niasari M (2017) Enhancement of magnetic, electrochemical and photocatalytic properties of lead hexaferites by coating graphene and CNT: sol-gel auto-combustion synthesis by valine. *Sep Purif Technol* 185:140–148
- Mahdiani M, Soofivand F, Ansari F, Salavati-Niasari M (2018) Grafting of CuFe₁₂O₁₉ nanoparticles on CNT and graphene: eco-friendly synthesis, characterization and photocatalytic activity. *J Clean Prod* 176:1185–1197
- Mul G, Zwijnenburg A, Van Der Linden B, Makkee M, Moulijn JA (2001) Stability and selectivity of Au/TiO₂ and Au/TiO₂/SiO₂ catalysts in propene epoxidation: an in situ FT-IR study. *J Catal* 201:128–137
- Narayanaswamy A, McBride J, Swafford LA, Dhar S, Budai JD, Feldman LC, Rosenthal SJ (2008) Synthesis and characterization of porous TiO₂ with wormhole-like framework structure. *J Porous Mater* 15:21–27
- Nasrollahzadeh M, Issaabadi Z, Sajadi SM (2018) Fe₃O₄@SiO₂ nanoparticle supported ionic liquid for green synthesis of antibacterially active 1-carbamoyl-1-phenylureas in water. *RSC Adv* 8(49):27631–27644
- Nasrollahzadeh M, Issaabadi Z, Sajadi SM (2019a) Green synthesis of Cu/Al₂O₃ nanoparticles as efficient and recyclable catalyst for reduction of 2,4-dinitrophenylhydrazine, Methylene blue and Congo red. *Compos B Eng* 166:112–119
- Nasrollahzadeh M, Issaabadi Z, Sajadi SM (2019b) Green synthesis of the Ag/Al₂O₃ nanoparticles using *Bryonia alba* leaf extract and their catalytic application for the degradation of organic pollutants. *J Mater Sci Mater Electron* 30(4):3847–3859
- Ojala S, Pitkääho S, Laitinen T, Koivikko NN, Brahmī R, Gaálová J, Matejova L, Kucherov A, Päivärinta S, Hirschmann C (2011) Catalysis in VOC abatement. *Top Catal* 54:1224–1256
- Park SJ, Das GS, Schütt F, Adelung R, Mishra YK, Tripathi KM, Kim T (2019) Visible-light photocatalysis by carbon-nano-onion-functionalized ZnO tetrapods: degradation of 2,4-dinitrophenol and a plant-model-based ecological assessment. *NPG Asia Mater* 11(1):8
- Pelaez M, Baruwati B, Varma RS, Luque R, Dionysiou DD (2013) Microcystin-LR removal from aqueous solutions using a magnetically separable composite N-doped TiO₂ catalyst under visible light irradiation. *Chem Commun* 49:10118–10120
- Salavati-Niasari M, Bazarganipour M (2007) Effect of single-wall carbon nanotubes on direct epoxidation of cyclohexene catalyzed by new derivatives of cis-dioxomolybdenum (VI) complexes with bis-bidentate Schiff-base containing aromatic nitrogen-nitrogen linkers. *J Mol Catal A Chem* 278(1–2):173–180
- Salavati-Niasari M, Bazarganipour M (2008) Covalent functionalization of multi-wall carbon nanotubes (MWNTs) by nickel (II) Schiff-base complex: synthesis, characterization and liquid phase oxidation of phenol with hydrogen peroxide. *Appl Surf Sci* 255(5):2963–2970
- Salavati-Niasari M, Bazarganipour M (2009) Synthesis, characterization and catalytic oxidation properties of multi-wall carbon nanotubes with a covalently attached copper (II) salen complex. *Appl Surf Sci* 255(17):7610–7617
- Salavati-Niasari M, Davar F, Bazarganipour M (2010) Synthesis, characterization and catalytic oxidation of para-xylene by a manganese (III) Schiff base complex on functionalized multi-wall carbon nanotubes (MWNTs). *Dalton Trans* 39(31):7330–7337
- Schmidt-Szałowski K, Krawczyk K, Sentek J, Ulejczyk B, Górská A, Młotek M (2011) Hybrid plasma-catalytic systems for converting substances of high stability, greenhouse gases and VOC. *Chem Eng Res Des* 89:2643–2651
- Sharma M, Joshi M, Nigam S, Shree S, Avasthi DK, Adelung R, Srivastava SK, Mishra YK (2019) ZnO tetrapods and activated carbon based hybrid composite: adsorbents for enhanced decontamination of hexavalent chromium from aqueous solution. *Chem Eng J* 358:540–551
- Szymański GS, Karpiński Z, Biniak S, Świątkowski A (2002) The effect of the gradual thermal decomposition of surface oxygen species on the chemical and catalytic properties of oxidized activated carbon. *Carbon* 40:2627–2639
- Tsumura T, Kojitani N, Umemura H, Toyoda M, Inagaki M (2002) Composites between photoactive anatase-type TiO₂ and adsorptive carbon. *Appl Surf Sci* 196:429–436
- Vandenbroucke AM, Morent R, De Geyter N, Leys C (2011) Non-thermal plasmas for non-catalytic and catalytic VOC abatement. *J Hazard Mater* 195:30–54
- Varshney G, Kanel SR, Kempisty D, Varshney V, Agrawal A, Sahle-Demessie E, Varma RS, Nadagouda MN (2016) Nanoscale TiO₂ films and their application in remediation of organic pollutants. *Coord Chem Rev* 306:43–64
- Vega AA, Imoberdorf GE, Mohseni M (2011) Photocatalytic degradation of 2,4-dichlorophenoxyacetic acid in a fluidized bed photo-reactor with composite template-free TiO₂ photocatalyst. *Appl Catal A Gen* 405:120–128
- Verma S, Nasir Baig RB, Nadagouda MN, Varma RS (2016) Titanium-based zeolitic imidazolate framework: chemical fixation of carbon dioxide. *Green Chem* 18:4855–4858
- Virkutyte J, Varma RS (2010) Fabrication and visible-light photocatalytic activity of novel Ag/TiO_{2-x}N_x photocatalyst. *New J Chem* 34:1094–1096
- Virkutyte J, Varma RS (2012a) Synthesis and visible light photoactivity of anatase Ag and garlic loaded TiO₂ nanocrystalline catalyst. *RSC Adv* 2:2399–2407
- Virkutyte J, Varma RS (2012b) Visible light activity of Ag-loaded and guanidine nitrate-doped nano-TiO₂: degradation of dichlorophenol and antibacterial properties. *RSC Adv* 2:1533–1539
- Virkutyte J, Baruwati B, Varma RS (2010) Visible light induced photobleaching of methylene blue over melamine doped TiO₂ nanocatalyst. *Nanoscale* 2:1109–1111
- Virkutyte J, Jegatheesan V, Varma RS (2012) Visible light activated TiO₂/microcrystalline cellulose nanocatalyst to destroy organic contaminants in water. *Bioresour Technol* 113:288–293
- Wang S, Zhou S (2011) Photodegradation of methyl orange by photocatalyst of CNTs/P-TiO₂ under UV and visible-light irradiation. *J Hazard Mater* 185:77–85
- Wang Q, Liang X, Qiao W, Liu C, Liu X, Zhan L, Ling L (2009a) Preparation of polystyrene-based activated carbon spheres with

- high surface area and their adsorption to dibenzothiophene. *Fuel Process Technol* 90:381–387
- Wang X, Liu Y, Hu Z, Chen Y, Liu W, Zhao G (2009b) Degradation of methyl orange by composite photocatalysts nano-TiO₂ immobilized on activated carbons of different porosities. *J Hazard Mater* 169:1061–1067
- Wetchakun N, Phanichphant S (2008) Effect of temperature on the degree of anatase-rutile transformation in titanium dioxide nanoparticles synthesized by the modified sol–gel method. *Curr Appl Phys* 8:343–346
- Williams G, Kamat PV (2009) Graphene-semiconductor nanocomposites: excited-state interactions between ZnO nanoparticles and graphene oxide. *Langmuir* 25:13869–13873
- Yang X, Zhang X, Ma Y, Huang Y, Wang Y, Chen Y (2009) Superparamagnetic graphene oxide-Fe₃O₄ nanoparticles hybrid for controlled targeted drug carriers. *J Mater Chem* 19:2710–2714
- Yang L, Luo S, Li Y, Xiao Y, Kang Q, Cai Q (2010) High efficient photocatalytic degradation of *p*-nitrophenol on a unique Cu₂O/TiO₂ pn heterojunction network catalyst. *Environ Sci Technol* 44:7641–7646
- Yap PS, Lim TT, Srinivasan M (2011) Nitrogen-doped TiO₂/AC bi-functional composite prepared by two-stage calcination for enhanced synergistic removal of hydrophobic pollutant using solar irradiation. *Catal Today* 161:46–52
- Yu JC, Yu J, Ho W, Jiang Z, Zhang L (2002) Effects of *F*-doping on the photocatalytic activity and microstructures of nanocrystalline TiO₂ powders. *Chem Mater* 14:3808–3816
- Yue X, Zhang R, Zhang F, Wang L (2010) Decomposition of crude oil absorbed into expanded graphite/TiO₂/NiO composites. *Desalination* 252:163–166
- Zarezade M, Ghasemi S, Gholami MR (2011) The effect of multi-walled carbon nanotubes and activated carbon on the morphology and photocatalytic activity of TiO₂/C hybrid materials. *Catal Sci Technol* 1:279–284
- Zeng J, Liu S, Cai J, Zhang L (2010) TiO₂ immobilized in cellulose matrix for photocatalytic degradation of phenol under weak UV light irradiation. *J Phys Chem C* 114:7806–7811
- Zhang X, Zhou M, Lei L (2005) Preparation of photocatalytic TiO₂ coatings of nanosized particles on activated carbon by AP-MOCVD. *Carbon* 43:1700–1708
- Zhao M, Liu P (2009) Adsorption of methylene blue from aqueous solutions by modified expanded graphite powder. *Desalination* 249:331–336

Publisher's Note Springer Nature remains neutral with regard to jurisdictional claims in published maps and institutional affiliations.

Affiliations

Babak Jaleh¹ · Mastaneh Gandomi Rouzbahani¹ · Kamaladdin Abedi^{2,3} · Saeid Azizian⁴ · Hossein Ebrahimi⁵ · Mahmoud Nasrollahzadeh⁶  · Rajender S. Varma⁷ 

¹ Department of Physics, Faculty of Science, Bu-Ali Sina University, Hamedan 65174, Iran

² Lung Diseases and Allergy Research Center, Kurdistan University of Medical Sciences, Sanandaj, Iran

³ Department of Occupational Health Engineering, Faculty of Health, Kurdistan University of Medical Sciences, Sanandaj, Iran

⁴ Chemistry Faculty, Bu-Ali Sina University, Mahdijeh Street, Hamedan, Iran

⁵ Air Pollution Research Center, School of Public Health, Iran University of Medical Sciences (IUMS), Tehran, Iran

⁶ Department of Chemistry, Faculty of Science, University of Qom, P.O. Box 37185-359, Qom, Iran

⁷ Department of Physical Chemistry, Faculty of Science, Regional Centre of Advanced Technologies and Materials, Palacky University, Šlechtitelů 27, 783 71 Olomouc, Czech Republic